The Indian Ocean SST Link to Solar Induced Chlorophyll Fluorescence Over India During Early Summer Monsoon

Roma Varghese
Indian Institute of Technology Kharagpur
Swadhin K. Behera
Japan Agency for Marine-Earth Science and Technology
Mukunda Dev Behera (mdbehera@coral.iitkgp.ac.in)
Indian Institute of Technology Kharagpur

Research Article

Keywords: sea surface temperature (SST), The Indian Ocean, Chlorophyll Fluorescence, Early Summer Monsoon, India

Posted Date: December 6th, 2021

DOI: https://doi.org/10.21203/rs.3.rs-1133874/v1

Abstract

This is a maiden attempt to explore the influence of sea surface temperature (SST) variations in the tropical Indian Ocean on the gross primary productivity (GPP) of the terrestrial vegetation of India during the summer monsoon. We studied the productivity of the vegetation across India using solar-induced chlorophyll fluorescence (SIF) as a proxy. Our results demonstrated a strong negative SST–SIF relationship: the productivity decreases (increases) when the SST of the tropical Indian Ocean is higher (lower) than normal. This SST–SIF coupling observed during June can be explained through the atmospheric teleconnections. Positive SST anomalies weaken the land–ocean thermal gradient during the monsoon onset period, reduce the monsoon flow, and hence decrease the moisture transport from the ocean to the Indian mainland. The resultant water stress, along with the high air temperature, leads to a reduction in the GPP. Conversely, negative SST anomalies strengthen the monsoon and increase the availability of moisture for photosynthesis. There is scope for improving regional GPP forecasting studies using the observed SST–SIF relationships.

Introduction

Primary productivity plays a key role in the global carbon cycle as a considerable amount of atmospheric CO_2 gets locked up in terrestrial ecosystems through photosynthetic assimilations of carbon[1]. The gross primary productivity (GPP) of a terrestrial ecosystem is determined by the interaction of environmental characteristics, climate variables, and availability of nutrients[1]. The abiotic factors limiting plant productivity are the solar radiation reaching the earth's surface, availability of water and nutrients, and temperature[2]. As the atmospheric conditions indirectly affect the availability of nutrients to plants, climatic variables appear to have a dominant role in determining the photosynthetic efficiency of a terrestrial ecosystem[3]. However, the influence of the climate on productivity of the vegetation is neither simple nor direct. Due to the complexity of these processes and the dynamics involved, even small changes in climate systems bring about considerable changes in vegetation productivity across regional and global scales[4]. It is well known that climatic oscillations such as the El Niño Southern Oscillation (ENSO), Pacific Decadal Oscillation (PDO), and North Atlantic Oscillation (NAO) affect the global terrestrial primary productivity through teleconnections[5]. Even though many studies have explained the response of terrestrial ecosystems to different climate drivers, the effect of sea surface temperature (SST) on terrestrial productivity has largely remained unexplored.

The SST strongly influences the atmospheric circulation and potentially affects the vegetation productivity by modulating the precipitation and temperature patterns on land. There are shreds of evidence to show that there is significant ocean–land connectivity across different parts of the globe and to prove the relevance of the SST in the functioning of terrestrial ecosystems[6,7]. SST fluctuations in the West Pacific Warm Pool have a strong but variable influence on the plant productivity in both the northern and southern hemispheres[8]. The vegetation greenness of the arid and semi-arid climatic zones in the tropics is tightly linked to oceanic variations. Enhanced vegetation indices may be predicted 3–6 months ahead using SST[9]. A monthly 100-year output of the coupled CCM3-IBIS model shows that the SSTs of the major oceans are correlated to the net primary production (NPP) of South American vegetation, in current and future scenarios[10]. Similarly, the variability of the normalized difference vegetation index (NDVI) in semi-arid regions of the Sahel exhibited was significantly related to global SST anomalies[11]. The influence of local SST changes persists in the spatial variability of the GPP in water-limited ecosystems[12]. Most studies have considered vegetation indices to represent ecosystem functionality; but this does not represent the actual amount of carbon taken in by the vegetation. Moreover, there are errors in these greenness-based indices due to radiometric saturation, background reflection, and environmental stresses[13–16].

A newly developed satellite-derived data called solar-induced chlorophyll fluorescence (SIF) serves as a better indicator of GPP[17]. SIF is the energy flux in the red and far-red band of the electromagnetic spectrum from chlorophyll molecules excited during photosynthesis. The captured photons show the status of actual photosynthesis, thus helping gain a clearer understanding of terrestrial carbon dynamics[18,19]. Spectrometers originally designed for atmospheric chemistry applications now generate global SIF datasets using Fraunhofer lines[20]. The use of SIF overcomes some of the limitations of conventional vegetation indices[21] as it avoids extrapolating the GPP, which may fail to capture transient stresses[22]. Since SIF effectively indicates the vegetation water stress[23], the variations in the rainfall and the associated changes in the photosynthetic assimilation of carbon may also

be inferred from the variations in the SIF. Thus, there is considerable potential for using satellite-based high-resolution SIF products to continuously monitor the GPP of terrestrial ecosystems and how they respond to climate change.

As India is the fourth largest emitter of CO_2, one of the harmful greenhouse gases responsible for global warming, it is vital to understand the terrestrial ecosystem carbon fluxes in the country. The GPP in India varies from 0 to 4147.55 g C m^{-2} $year^{-1}$, with a mean of 1507.32 g C m^{-2} $year^{-1}$, and 142.68 g C m^{-2} $month^{-1}$ is fixed during the summer monsoon according to estimates generated for the year 2008[24]. The average Indian GPP varies between 2.9 and 3.3 Pg C yr^{-1}. Studies have confirmed the sensitivity of the terrestrial carbon cycle to climate change and indicated that any variations in atmospheric conditions could impact ecosystem services[25,26]. Besides, large-scale modes of climate variability such as ENSO affect the vegetation productivity across India, which indicates the relevance of both ocean and atmospheric characteristics to the functionality of terrestrial ecosystems[27,28]. Thus there is scope for extending the investigation of climate–vegetation interactions by incorporating oceanic variables.

SST, the critical climate indicator that provides information about the ocean surface heat, is a key element that determines the earth's climate[29]. The influence of SST variations is directly visible in the climatic conditions: SST, in conjunction with surface air temperatures, creates extreme climate phenomena that result in significant economic and agricultural losses[30]. Since the variability of monsoon rainfall is associated with the heat content of the surface waters of the tropical Indian Ocean[31], any fluctuation in the SST may affect the functioning of terrestrial vegetation ecosystems in India.

The Indian Ocean is physically the most complex of the world's three major oceans[32]. The differential heating between land and ocean creates a seasonally reversing monsoonal wind and ocean circulation in the region[33]. The strong meridional pressure gradient produced during the boreal summer monsoon forces a southwesterly wind from the Indian Ocean[34]. However, the role of the Indian Ocean in the variability of the monsoon rainfall is complex, even though the ocean is an important modulator of tropical climate variability[35,36]. In addition to the teleconnections with the Pacific Ocean, SST changes in the tropical Indian Ocean play a major role in Indian summer monsoon rainfall (ISMR) variability[37]. In India, several investigations have been carried to model the GPP using satellite-derived vegetation indices and their connections with climate parameters such as rainfall, solar radiation, and temperature[25,38,39], but the impact of SST on vegetation productivity remains unexplored. As phenomena like ENSO and the Indian Ocean Dipole (IOD) impact the tropical climate system[40,41], the previous investigations broadly evaluated the relationships between Indian vegetation productivity and these climate oscillations using the respective climate indices[42]. The Indian summer monsoon rainfall, which determines India's overall vegetation dynamics, is also intimately linked to the Indian Ocean SST variability since the temperature gradient between the ocean and land is the critical driving mechanism behind this coupled large-scale circulation[43–45]. Therefore the tropical Indian Ocean SST has a profound influence on the summer monsoon rainfall variability that is independent of the remote forcing induced by climate oscillations[46].

Thus the current study aims to unveil the relationship between the regional-scale variability of the tropical Indian Ocean SST and the Indian vegetation productivity to identify regions with strong SST–GPP coupling during the summer monsoon. SST was used as a climatic variable, and SIF was used as the GPP proxy to evaluate the ocean–vegetation intercommunication. To comprehensively understand the SST-SIF linkage, the Indian mainland was considered as 14 mainland agro-climatic zones (ACZs) such as Western Himalayan Region (WHR), Trans Gangetic Plains (TGP), Upper Gangetic Plains (UGP), Middle Gangetic Plains (MGP), Lower Gangetic Plains (LGP), Eastern Himalayan Region (EHR), Western Dry Region (WDR), Central Plateau and Hills (CPH), Eastern Plateau and Hills (EPH), Gujarat Plain and Hills (GPH), Western Plateau and Hills (WPH), Southern Plateau and Hills (SPH), Western Coastal Plains and Ghats (WCPG), and Eastern Coastal Plains and Hills (ECPH)[47]. Likewise, the tropical Indian Ocean is divided into Western Indian Ocean (WIO), Northern Indian Ocean (NIO), and Central Indian Ocean (CIO).

Results

SIF and SST variations during the summer monsoon

The 18-year climatology of SIF indicates the spatial variability of the vegetation functional characteristics across India in the summer monsoon (Fig. 1). Overall, the magnitude of SIF varies by up to 0.55 W m^{-2} μm^{-1} sr^{1}. The EHR, which is dominated by thick forests of the northeastern region, appears to be the most productive ACZ, with a mean SIF of 0.35 W m^{-2} μm^{-1} sr^{-1}. The northwestern desert areas of WDR, characterized by sparse vegetation and an arid climate, are the least productive area and thus show weak SIF signals (0.05 W m^{-2} μm^{-1} sr^{-1}). Details of the estimated SIF are provided in Table S1. Fig. 2 shows the distribution of SIF values during the monsoon months: the photosynthesis rate is lowest in June and highest in August. During the monsoon's initial stages, the maximum SIF values are in the forest areas, while they are comparatively low in croplands. The contribution of the croplands to the total productivity of the vegetation in India increases rapidly once the monsoon attains its peak in August. The magnitude of the SIF of the forest ecosystems across the country remains roughly the same even in the second half of the monsoon, and the SIF variability in August and September is nearly the same. There is a significant intraseasonal oscillation in this SIF pattern. Overall, the ACZs in the Indo-Gangetic Plains and the central Indian region display the highest variability in productivity due to significant interannual and intraseasonal changes in the monsoon rainfall at these locations.

The tropical Indian Ocean SST exhibits a unique regional distribution based on an 18-year monthly climatology of the summer monsoon. The SSTs of the western, northern, and central Indian Ocean (WIO, NIO, and CIO) have ranges of 26.78–30.22°C, 23.33–29.53°C, and 21.91–28.26°C, respectively (Fig. 1). NIO is the warmest, followed by WIO and CIO. The de-trended time series of mean monthly SST anomalies during the monsoon period exhibits large interannual variability in each of the oceanic regions (Fig. 3). The maximum SST anomalies observed are in WIO, followed by NIO and CIO. The SST fluctuations of WIO and NIO are closely linked (+0.80), although the variations of CIO diverge slightly (Fig. 3-a). The time series of indices such as SST anomalies in the NINO3 region (NINO3), the dipole mode index (DMI), and difference between the western and central India Ocean SSTs (W-CIO) represent the possible influence of climate events (ENSO and IOD) on the SST variations in individual Indian Ocean regions (Fig. 3-b). The DMI shows a considerable correlation strength with the SST anomalies in both WIO and NIO as well as the W-CIO. Relatively, the degree of correlation between the index NINO3 and the three Indian Ocean regions appears to be weaker.

Linear SST-SIF correlations

The correlations between the SST anomalies in the three Indian Ocean regions and the SIF anomalies in the 14 ACZs were computed for June, July, August, and September. As per the statistics, the strengths of the SST–SIF associations vary both spatially and temporally (Table 1). Overall, the Pearson correlation coefficient reached the maximum value of -0.74, between CIO and CPH in June. Only the robust SST–SIF connections, which are statistically significant, were evaluated. Broadly, the SIF anomalies of all the ACZs except EHR appear to be impacted by SST variations in at least one Indian Ocean region during one of the monsoon months. The SST anomalies in June in WIO show strong correlations with the SIF variability of ECPH (-0.55), EPH (-0.60), SPH (-0.48), CPH (-0.55), TGP (-0.56), UGP (-0.59), and WHR (0.53), while the correlations with the SIF variabilities in August in WCPG and LGP were +0.58 and -0.48, respectively. When the monsoon ends in September, WIO shows a strong correlation with WCPG (+0.59), TGP (0.47), and WDR (-0.51). The coefficients of the correlation of the SIF anomalies of EPH, CPH, TGP, UGP, MGP, and WHR with the SST anomalies in NIO in June are -0.53, -0.60, -0.48, -0.54, -0.55, and -0.50. Strong SST–SIF links are observed only between NIO and WCPG in August (+0.65) and in September (+0.50). Similarly, at the onset of the monsoon, the CIO SST anomalies are linked to the SIF anomalies of EPH (-0.68), WPH (-0.66), CPH (0.74), TGP (-0.50), UGP (-0.55), MGP (-0.55), GPH (-0.60), and WHR (-0.54). These ACZs cover the entire Deccan Plateau except for the southern parts, the full stretch of the Indo-Gangetic Plains, and the hot and cold deserts of India. When the monsoon peaks in August, the teleconnections with the CIO SST anomalies are confined to the arid regions of GPH (+0.59) and WDR (+0.51), on the western Indian boundary. As the monsoon withdraws, the CIO SST influence shifts to ECPH (+0.53) and EPH (+0.48), of eastern coastal India.

Table 1
The correlation coefficients (r) between SST and SIF during the months of June, July, August and September, mentioned across the western, northern and central Indian Ocean. The statistically significant at P<0.05 correlations are shown in bold tests

	Correlation Coefficient (r)											
Agro Climatic zone	Western Indian Ocean (WIO)				Northern Indian Ocean (NIO)				Central Indian Ocean (CIO)			
	Jun	Jul	Aug	Sep	Jun	Jul	Aug	Sep	Jun	Jul	Aug	Sep
WCPG	-0.415	-0.066	**0.581**	**0.593**	-0.083	-0.051	**0.649**	**0.495**	-0.296	-0.375	-0.045	0.398
ECPH	**-0.549**	-0.142	0.062	0.216	-0.196	-0.077	0.201	0.262	-0.227	0.147	0.292	**0.533**
EPH	**-0.609**	-0.207	0.125	0.042	**-0.534**	-0.313	0.205	0.141	**-0.676**	-0.241	0.084	**0.475**
WPH	-0.222	0.187	-0.041	-0.332	-0.325	0.061	0.011	-0.270	**-0.657**	0.266	0.394	-0.061
SPH	**-0.478**	0.005	-0.159	0.037	-0.245	0.0003	-0.037	0.145	-0.295	0.262	0.317	0.387
CPH	**-0.546**	-0.122	0.005	-0.337	**-0.607**	-0.166	0.163	-0.177	**-0.738**	0.151	0.425	0.008
TGP	**-0.559**	-0.220	-0.368	**-0.472**	**-0.476**	-0.167	-0.184	-0.141	**-0.494**	0.210	0.382	0.129
UGP	**-0.593**	-0.342	-0.115	-0.087	**-0.540**	-0.343	0.071	-0.328	**-0.546**	-0.017	0.116	-0.120
MGP	-0.443	-0.401	-0.201	0.219	**-0.557**	-0.407	-0.016	0.288	**-0.554**	-0.133	-0.290	0.280
LGP	-0.322	-0.445	**-0.481**	-0.388	-0.282	-0.372	-0.109	0.090	-0.317	-0.016	-0.267	0.351
GPH	-0.291	0.119	-0.365	-0.433	-0.387	0.036	-0.137	-0.104	**-0.607**	0.191	**0.592**	0.376
WDR	-0.408	0.181	-0.280	**-0.512**	-0.396	0.122	-0.031	-0.149	-0.412	0.228	**0.505**	0.270
WHR	**-0.526**	-0.400	-0.095	0.057	**-0.501**	-0.381	0.391	0.206	**-0.536**	-0.029	0.453	0.258
EHR	-0.177	-0.063	-0.369	-0.449	-0.374	-0.121	-0.229	-0.383	-0.128	0.277	0.227	-0.057

ENSO and IOD teleconnections

To isolate the effects of ENSO and the IOD, a partial correlation was calculated between SST and SIF. Only the partial correlation between the oceanic regions and ACZs having significant linear correlation coefficients are discussed here (Table 2). Compared with the standard linear correlations (Table 1), the strength of the SST–SIF association does not decrease greatly even with the removal of the influences of ENSO and the IOD, and some of those relationships remained statistically significant, indicating that the influences of ENSO and the IOD are not very significant. All the ACZs other than the highlighted ones linked with the tropical Indian Ocean regions. Based on the estimated partial correlations, the intensity of the ENSO and IOD effects on the SIF variability across India is less in June, but it gradually increases as the monsoon proceeds. Even after excluding the independent effect of ENSO and the IOD from the respective months, most of the productive ACZs across northern and central-eastern portions of India maintained their relationship with WIO in June. Similarly, the significance of the NIO SST anomalies is still considerable in EPH, CPH, UGP, and MGP, whereas the CIO has maintained its SST teleconnection with all of the selected ACZs except TGP. No considerable ocean–land connectivity is observed in August and September, during which period the WIO SST anomalies are linked with the SIF variability across India. Besides, in August both NIO and CIO show significant connections only with WCPG and GPH, respectively. During September, the linkage of the CIO SST shifts to the SIF anomalies of ECPH and LGP. However, there may still be certain ambiguities in the reported SST–SIF correlations (e.g., interactive effects of ENSO and IOD when they coincide). The composite of SIF anomalies (Fig. 4), on the other hand, illustrates how India's terrestrial ecosystems respond to severe positive and negative SST years in the western, northern, and central Indian Oceans, thus clearly representing the independent influence of the tropical Indian Ocean SST on the Indian vegetation productivity.

Table 2
Partial Correlation coefficient determined to understand the independent influence of SST fluctuations in Indian Ocean basins over the months of June, August and September, where SST anomalies due to ENSO and IOD events kept as fixed variables. The highlighted Agro-climatic zones contain the impact of climatic oscillations in the observed SST-SIF relationship.

Partial Correlation coefficient between Indian Ocean SST and SIF limiting NINO3 SST									
Oceanic	June			August			September		
region	ACZ	Independent variables		ACZ	Independent variables		ACZ	Independent variables	
		NINO3	DMI		NINO3	DMI		NINO3	DMI
WIO	**ECPH**	-0.55	**-0.38**	**WCPG**	+0.51	**+0.16**	**WCPG**	+0.58	**+0.316**
	EPH	-0.63	-0.56	**LGP**	-0.59	**-0.32**	**TGP**	**-0.37**	**-0.69**
	CPH	-0.56	-0.66				**WDR**	**-0.34**	**-0.72**
	SPH	-0.49	**-0.37**						
	TGP	-0.57	-0.59						
	UGP	-0.62	-0.52						
	WHR	-0.55	-0.50						
NIO									
	EPH	-0.51	-0.49	WCPG	+0.59	+0.54	**WCPG**	**+0.46**	**+0.24**
	CPH	-0.58	-0.65						
	TGP	**-0.44**	**-0.47**						
	UGP	-0.51	-0.49						
	MGP	-0.52	-0.52						
	WHR	**-0.46**	**-0.47**						
CIO									
	EPH	-0.66	-0.72	GPH	+0.55	+0.58	ECPH	+0.55	+0.48
	WPH	-0.65	-0.66	**WDR**	**+0.46**	+0.53	EPH	+0.53	+0.48
	CPH	-0.72	-0.74						
	TGP	**-0.463**	-0.50						
	UGP	-0.51	-0.59						
	MGP	-0.52	-0.58						
	GPH	-0.58	-0.61						
	WHR	-0.50	-0.56						

The link of SIF variations over India with Indian Ocean SST during early monsoon

The inverse ocean-land linkage observed in the correlation analyses is also seen in the composite anomalies of SIF. It indicates that the plant productivity in India declines when the WIO, NIO, and CIO are warmer than normal (Fig. 4i-a,b,c). Similarly, the influence of colder-than-normal surface waters in the same oceanic regions enhances plants' photosynthetic rates, as displayed by the positive anomalies of SIF (Fig. 4i-d,e,f). However, apart from the results obtained in the correlation analysis, some other

ACZs are also influenced by SST variations in the WIO. This predominantly includes MGP and WPH. Overall, the effect of the WIO warm anomaly is concentrated on ACZs such as WHR, TGP, UGP, MGP, EPH, WPH, and CPH (Fig. 4i-a). But the influence of NIO's SST is confined to the ACZs that lie in the north-central areas (Fig. 4i-b&e). As per the SST–SIF correlations, the NIO governs the vegetation productivity only in the EPH, CPH, UGP, and MGP. The composite analysis reveals that WHR and TGP are also subject to the effect of SST signals from the NIO. However, the oceanic influence extends over the same geographical extent in both analyses. The SST patterns in the western and central oceanic regions are nearly identical, as illustrated in Fig. 1. This similarity is also observed in the SST teleconnections to SIF anomalies all over India. The influence of CIO is predominantly found in the Indo-Gangetic Plains and the northern and central regions of India (Fig. 4i-c&f). As with the SST interactions from WIO, the SST anomalies in CIO govern the plant production in EPH, CPH, UGP, and WHR. Furthermore, GPH, WPH, and MGP also showed linkages to the CIO SST. The composites of SIF anomalies almost agree with the observed correlation with the SST (Table 2).

The linkage between the Indian ecosystem and the tropical Indian Ocean was examined using composite anomalies of the important hydroclimatic variables (specific humidity, rainfall, and soil moisture) and the air temperature. These auxiliary parameters indicate how the SST variations in WIO, NIO, and CIO are connected with the functionality of the terrestrial ecosystem through modulation of the availability of water to the plants for photosynthesis. The composite of specific humidity (Fig. S1), rainfall (Fig. S2), soil moisture (Fig. S3), and air temperature (Fig. S4) showed corresponding anomalies that agree with the SIF pattern according to the warm and cold SST anomalies. Negative anomalies of the specific humidity (Fig. S1-a,b,c), rainfall (Fig. S2-a,b,c), and soil moisture (Fig. S3-a,b,c), together with positive air temperature anomalies (Fig.S4-a,b,c) across India, result in negative anomalies of SIF because the corresponding water stress reduces the vegetation productivity as the surface waters of WIO, NIO, and CIO are warmer than normal. Similarly, negative anomalies of air temperature (Fig. S4-d,e,f), together with positive anomalies of specific humidity (Fig. S1-d,e,f), rainfall (Fig.S2- d,e,f), and soil moisture (Fig.S3- d,e,f), occur due to negative SST anomalies, which reduces the chances of the vegetation experiencing water stress and favour positive SIF anomalies. Except for WHR, all the agro-meteorological metrics studied here show corresponding anomalies that match the SIF pattern on the same terrestrial band and are limited mainly to the northern Indian regions when the NIO is warmer than normal, while the central-eastern side of India exhibits considerable anomalies of these hydroclimatic variables when negative SST anomalies persist in the NIO. Comparatively, the positive SIF anomalies induced by the negative CIO SST anomalies are weaker across India (Fig. 4i-f). This effect is also observed in the variation of agro-climatic parameters (Fig. S1-f, S2-f, S3-f, S4-f). Thus the viability of the identified SST–SIF links is clear when there is a warm anomaly in the CIO, but it is less evident when the anomaly is a cold. Overall, the results suggest that the relationship between SST variations in the western, northern, and central Indian Ocean and SIF anomalies across India is feasible through atmospheric teleconnections.

The SST–SIF link after June

The ocean–terrestrial vegetation interactions observed in June appear to deteriorate thereafter, which points to the complexity of the physical processes associated with the later phase of the summer monsoon. Only a few strong SST–SIF correlations are seen during August and September in the analyses. The negative SST–SIF correlation observed in June shifts to a mixed kind of relationship in August and September (Table 1). But mostly, a positive SST–SIF relationship was observed during this phase of the summer monsoon. Apart from the SST–SIF associations identified in partial correlation analysis, the positive effect of SST anomalies from Indian Ocean regions slightly influences the vegetation productivity of some other terrestrial ecosystems across India (Fig. 4ii&4iii). However, the cause–effect chain of SST and SIF failed in August (Fig. S5-S8) and September (Fig. S9 & S10) as the observed composite anomalies are not significant.

Discussion

Our findings give another dimension to the impact of climate on the Indian terrestrial ecosystem by incorporating teleconnections stemming from SST variations in the tropical Indian Ocean. As the SST exerts a major influence on the air–sea interactions, it drives the global weather systems and climate patterns. Therefore changes in the SST, either increases or decreases, can cause a wide variety of impacts in every component of the climate system. The vegetation carbon dynamics across India mainly depends on seasonally occurring rainfall events, especially the summer monsoon, which is linked to the regional SST variations in the Indian Ocean. Therefore, it is expected that the vegetation productivity in India is linked to the SST

variability in the Indian Ocean. This is correct at a seasonal scale, and we investigated the details by stratifying the monsoon season into individual months (June, July, August, and September). The idea behind the stratified analysis was to understand the intra-seasonal variability of the SST–SIF relationship rather than establish a general relationship for a season. Indeed, as expected, a strong SST–SIF link was found only in the early monsoon period. Therefore, the rest of this discussion is mostly based on the June SST–SIF relationship.

The inverse nature of the SST–SIF relationship in June indicates that vegetation productivity reacts opposite to SST changes. Warmer SST anomalies in the tropical Indian Ocean regions reduce the land–sea thermal gradient and lead to the weakening of the monsoon circulation, thus producing negative anomalies of rainfall across India[48]. The weakened southwesterly wind is also evident in the composite anomalies of wind speed vectors over the entire study area (Fig. S11), and it hinders the moisture transport from the tropical Indian Ocean, as depicted by northeasterly anomalies. The consequent reduction in rainfall and soil moisture and the increase in air temperature create water stress in plants, which decreases the vegetation productivity[49–51]. Similarly, cold SST anomalies in the Indian Ocean generate a strong land–sea gradient and increase the monsoon activity. The relatively strong summer monsoon winds blowing from southwest of the tropical Indian Ocean region (Fig. S12) bring an ample amount of water to India. The resultant positive rainfall anomalies generate positive anomalies of soil moisture, reduce the chances of water stress together with cooler air temperature anomalies, and, therefore, enhance the vegetation productivity. The Indian Ocean is warming in response to global warming, and the impact of this warming through atmospheric teleconnections should reflect in the functional characteristics of terrestrial vegetation. An attempt is made to infer such a possibility on the basis of the present analyses though no attempt has been made here to understand the influence of the Indian Ocean warming trend. It was found that the warmer years of the Indian Ocean are more influential as compared with the cooler years, indicating a bias of the SST–SIF link to warmer trends. This means a warmer Indian Ocean will lead to reduced GPP across India, at least in the initial phase of the monsoon. Consequently, the decline in vegetation primary production probably will alter the land–atmosphere–ocean interactions and affects the climate over the Indian subcontinent. A drop in GPP will adversely affect plant health, reducing crop yields and raising concerns about food security. This may result in significant socio-economic issues in India along with environmental impacts.

Overall, the SST effect was observed mostly in the plant productivity across the central and northern Indian regions, where the land largely comprises rain-fed agricultural lands and forest ecosystems, the NPP of which areas fluctuates according to the monsoon rainfall[52,53]. Mostly an arid–semi arid climatic condition persists in the ACZs of this region and, in some areas, shifts to sub-humid climates. Normally, the hydrologic fluctuations control the vegetation growth in arid to semi-arid ecosystems[54,55]. Especially in regions that are predominantly covered with rain-fed agricultural lands, the crop productivity depends on the precipitation as a source[56]. Additionally, the net primary productivity of the forest ecosystems in the tropical belt depends to a large extent on the precipitation[57].

The inverse relationship between the SST and GPP in June decouples afterward. No significant relationship is found for July, which could be because of the fact that the rainfall impacts are already factored into the vegetation growth in June. Even though the composite of SIF exhibits positive anomalies in August and September, their intensities, as well as spatial coverage, are much smaller compared with the onset phase. This is because once the monsoon establishes over the country in June, convective heating plays a major role in maintaining the tropospheric temperature gradient and the monsoon circulation during the remaining months[58]. The recharge of soil water during the initial phase of the monsoon helps the atmospheric moisture from terrestrial sources to become more active through evapotranspiration and contributes significantly to the Indian summer monsoon. Therefore the decoupling the SST–SIF relationship after the onset phase of the monsoon could be due to the establishment of more local circulations owing to terrestrial moisture build-ups and/or the effects of local interference. The present study focused mostly on the nature of the SST–GPP relationship, but there are other factors within the ocean–atmosphere–vegetation interactions, especially during the monsoon. In the future, the authors will investigate these uncertainties comprehensively and figure out how the SST–GPP connection works throughout the monsoon. The contribution of the SST to the vegetation productivity suggests the possibility of prediction, which may facilitate improved GPP forecasts in India. Such forecasts are beneficial to forest management practices, and the efficient use of water resources in croplands. They also contribute to the understanding of future imbalances in the Indian terrestrial carbon budget arising from climate change.

Methodology

India is a mega-diverse country that spans latitudes 8–38°N and longitudes 66–100°E (Fig. 1). It has an extent of over 3.287 million km^2, of which 44.12% is cultivated land. The country is primarily guarded by the Himalaya in the north and surrounded by the Indian Ocean on the other three sides. The 20.39% forest cover includes deciduous broad-leaved, deciduous needle-leaved, evergreen broad-leaved, evergreen needle-leaved, and mangrove forests, along with shrubland and grassland[59]. The climate of the country varies from monsoonal to temperate, with complex agro-climatic situations. The country has been divided into different (homogeneous) ACZs on the basis of physiography, soil, climate, and vegetation by the Indian Planning Commission[60]. India experiences the summer monsoon, or southwest monsoon, during June, July, August, and September. This monsoon brings torrential rainfall to the mainland[61]. Since the major portion of India's vegetation relies on the monsoon rainfall, its variability at any scale has a considerable influence on the terrestrial carbon dynamics as well as the food security of the country.

Gridded global datasets of SIF, SST, wind components, specific humidity, rainfall, soil moisture, and air temperature collected during 2001–2018 were used (Table 3). Global Orbiting Carbon Observatory SIF (GOSIF) version 2 data were developed by integrating coarser Orbiting Carbon Observatory-2 (OCO-2) SIF, surface reflectance from the Moderate Resolution Imaging Spectroradiometer (MODIS) and reanalysis meteorological data from the Modern-Era Retrospective Analysis for Research and Applications (MERRA-2) using machine learning methods[62]. These SIF estimates are highly correlated with GPP from 91 FLUXNET sites[63,64]. SST data were collected from the NOAA 0.25° daily Optimum Interpolation Sea Surface Temperature version 2 (OISST V2) high-resolution product[65]. The dataset was constructed by combining observations from different platforms (satellites, ships, buoys, and Argo floats)[66]. The U and V wind components were collected from the European Centre for Medium-Range Weather Forecasts (ECMWF) reanalysis dataset[67]. To represent the influence of ENSO, the SST anomalies in the Nino 3 region were derived using the area-averaged SST data obtained from the global climate observing system of Physical Sciences Laboratory (PSL)[68]. The intensity of the IOD is represented by the anomalous SST gradient between the western equatorial Indian Ocean and the southeastern equatorial Indian Ocean, represented by DMI. DMI values were also obtained from the monthly climate time series provided by PSL[69]. We used high-resolution daily rainfall data from the India Meteorological Department. Soil moisture data were obtained from the FEWS NET land data assimilation system model output[70]. We used specific humidity values at a pressure level of 850 hPa and air temperature at 2 m height, from the MERRA-2 model[71].

Table 3
Details of data used during 2001 to 2018 at monthly temporal resolution

Data	Spatial Resolution (Deg)	Source
Solar-Induced chlorophyll Fluorescence	0.05 x 0.05	GOSIF V2
Sea Surface Temperature	0.25 x 0.25	NOAA OISST V2.1
Air Temperature at 2m	0.5 x 0.625	MERRA-2 Model
Specific humidity at 850hPa	0.5 x 0.625	MERRA-2 Model
Rainfall	0.25 x 0.25	IMD
Wind components at 850hPa	0.25 x 0.25	ERA5
Soil Moisture	0.1 x 0.1	FLDAS Model
NINO3 SST and DMI	-	NOAA PSL GCOS

All the datasets were converted to 0.05° × 0.05° gridded data after being processed to a monthly scale. The SST indices were derived for the WIO, NIO, CIO, and the difference between the western and central India Ocean (W-CIO) by taking area averages over those domains. The geographical extent of WIO, NIO, and CIO along with the 14 ACZs is given in Fig. 1. The wind speed at 850 hPa was calculated using the formula

Wind speed=$\sqrt{u^2 + v^2}$, where *u* and *v* are the zonal and meridional components of the wind, respectively.

An outline of the methodology adopted in this study is provided in Fig. 5. The 18-year climatology was generated for all the collected datasets and the anomalies during each year in June, July, August, and September were calculated from it. A de-trended time series was generated for the SST anomalies in each of the three demarcated regions in the Indian Ocean and for the SIF anomalies in the 14 ACZs separately. Moreover, the W-CIO index was derived from the difference in SST between the western and central parts of the Indian Ocean. To represent the interactions related to the climate events, the de-trended time series of NINO3, W-CIO, and DMI was also incorporated in the analysis. The Pearson correlation coefficient was determined for all the combinations of the SST and SIF anomalies. To exclude the influence of SST anomalies forced by the ENSO and IOD events, a partial correlation between the SST anomalies in the Indian Ocean and the SIF anomalies in the ACZs was calculated. To obtain better clarity about the impact of SST variations on the Indian climate and vegetation as well as to understand the route of the SST–SIF connectivity, composites of the anomalies were made. These were made for the years in which the anomalies in the SST in the Indian Ocean were above and below +0.5°C and -0.5°C (WIO) and +0.25°C and -0.25°C (NIO and CIO). These criteria were selected on the basis of the 75th percentile of the representation of extreme SST events. All the composite anomalies were tested for statistical significance at the 95% confidence level using the two-tailed Student's *t*-test.

Declarations

Author contributions

Conceptualization, R.V., M.D.B. and S.B.; Formal analysis; Methodology, R.V., M.D.B. and S.B.; supervision, S.B. and M.D.B.; Writing—original draft, R.V.; writing—review and editing, S.B. and M.D.B.. All authors have read and agreed to the content of the manuscript

Competing interests

The authors declare no competing interest

Data availability

The GOSIF is available at Global Ecology Group's data repository on reasonable request (http://data.globalecology.unh.edu/). OISST dataset is collected from National Centers for Environmental Information (https://www.ncei.noaa.gov/data/sea-surface-temperature-optimum-interpolation/v2/access/avhrr-only/). Rainfall data is available at the official site of the India meteorological department (https://www.imdpune.gov.in/Clim_Pred_LRF_New/Grided_Data_Download.html). Wind components are obtained from the C3S climate data store (https://cds.climate.copernicus.eu/cdsapp#!/dataset/reanalysis-era5-pressure-levels-monthly-means?tab=form). Soil moisture, specific humidity, and air temperature datasets are accessed via Giovanni (https://giovanni.gsfc.nasa.gov/giovanni/). Both Nino 3 SST index and dipole mode index were collected from climate time series developed by the GCOS surface pressure working group (https://psl.noaa.gov/gcos_wgsp/Timeseries/).

Code availability

The processing R and Python codes are available from the corresponding author upon request.

References

1. United States. Department of Energy. Office of Science. & United States. Department of Energy. Office of Biological and Environmental Research. *Carbon cycling and biosequestration integrating biology and climate through systems science: report from the March 2008 workshop*. (U.S. Dept. of Energy, Office of Science, Office of Biological and Environmental Research, Washington, DC, 2008).
2. Reichstein, M., Richardson, A. D., Migliavacca, M. & Carvalhais, N. *Plant-environment interactions across multiple scales*. *Ecology and the Environment* (2014). doi:10.1007/978-1-4614-7501-9_22.

3. Messori, G., Ruiz-Pérez, G., Manzoni, S. & Vico, G. Climate drivers of the terrestrial carbon cycle variability in Europe. *Environ. Res. Lett.* **14**, (2019).
4. Ayumah, R., Asante, F., Guodaar, L. & Eshun, G. How Do Climate and Nonclimatic Variables Influence the Production of Agricultural Staple Crops in Vulnerable Rural Communities in the Bawku Municipality of Northern Ghana? *Adv. Agric.* **2020**, 1–13 (2020).
5. Zhu, Z. *et al.* The effects of teleconnections on carbon fluxes of global terrestrial ecosystems. *Geophys. Res. Lett.* **44**, 3209–3218 (2017).
6. Los, S. O., Collatz, G. J., Bounoua, L., Sellers, P. J. & Tucker, C. J. Global interannual variations in sea surface temperature and land surface vegetation, air temperature, and precipitation. *J. Clim.* **14**, 1535–1549 (2001).
7. Kim, I. W. *et al.* Tropical Indo-Pacific SST influences on vegetation variability in eastern Africa. *Sci. Rep.* **11**, 1–8 (2021).
8. Huang, M. *et al.* Global vegetation productivity responses to the West Pacific Warm Pool. *Sci. Total Environ.* **655**, 641–651 (2019).
9. Yan, B. *et al.* Predictability of tropical vegetation greenness using sea surface temperatures. *Environ. Res. Commun.* **1**, 31003 (2019).
10. Pereira, M. P. S., Costa, M. H., Justino, F. & Malhado, A. C. M. Response of South American Terrestrial Ecosystems to Future Patterns of Sea Surface Temperature. *Adv. Meteorol.* **2017**, (2017).
11. Huber, S. & Fensholt, R. Analysis of teleconnections between AVHRR-based sea surface temperature and vegetation productivity in the semi-arid Sahel. *Remote Sens. Environ.* **115**, 3276–3285 (2011).
12. Reimer, J. J. *et al.* Sea surface temperature influence on terrestrial gross primary production along the southern California Current. *PLoS One* **10**, (2015).
13. Matsushita, B., Yang, W., Chen, J., Onda, Y. & Qiu, G. Sensitivity of the Enhanced Vegetation Index (EVI) and Normalized Difference Vegetation Index (NDVI) to topographic effects: A case study in high-density cypress forest. *Sensors* **7**, 2636–2651 (2007).
14. Tan, C. *et al.* Using hyperspectral vegetation indices to estimate the fraction of photosynthetically active radiation absorbed by corn canopies. *Int. J. Remote Sens.* **34**, 8789–8802 (2013).
15. Guanter, L. *et al.* Global and time-resolved monitoring of crop photosynthesis with chlorophyll fluorescence. *Proc. Natl. Acad. Sci. U. S. A.* **111**, (2014).
16. Behera, M. D. *et al.* Species-level classification and mapping of a mangrove forest using random forest—utilisation of avirising and sentinel data. *Remote Sens.* **13**, (2021).
17. Yang, K. *et al.* Sun-induced chlorophyll fluorescence is more strongly related to absorbed light than to photosynthesis at half-hourly resolution in a rice paddy. *Remote Sens. Environ.* **216**, 658–673 (2018).
18. Yang, X. *et al.* Solar-induced chlorophyll fluorescence that correlates with canopy photosynthesis on diurnal and seasonal scales in a temperate deciduous forest. *Geophys. Res. Lett.* **42**, 2977–2987 (2015).
19. Patel, N. R. *et al.* Estimating net primary productivity of croplands in Indo-Gangetic Plains using GOME-2 sun-induced fluorescence and MODIS NDVI. *Curr. Sci.* **114**, 1333–1337 (2018).
20. Mohammed, G. H. *et al.* Remote sensing of solar-induced chlorophyll fluorescence (SIF) in vegetation: 50 years of progress. *Remote Sens. Environ.* **231**, 111177 (2019).
21. Zhang, Z., Chen, J. M., Guanter, L., He, L. & Zhang, Y. From Canopy-Leaving to Total Canopy Far-Red Fluorescence Emission for Remote Sensing of Photosynthesis: First Results From TROPOMI. *Geophys. Res. Lett.* **46**, 12030–12040 (2019).
22. Chen, A. *et al.* Moisture availability mediates the relationship between terrestrial gross primary production and solar-induced chlorophyll fluorescence: Insights from global-scale variations. *Glob. Chang. Biol.* **27**, 1144–1156 (2021).
23. Ni, Z. *et al.* Assessing the response of satellite sun-induced chlorophyll fluorescence and MODIS vegetation products to soil moisture from 2010 to 2017: a case in Yunnan Province of China. *Int. J. Remote Sens.* **40**, 2278–2295 (2019).
24. Varghese, R. & Behera, M. D. Annual and seasonal variations in gross primary productivity across the agro-climatic regions in India. *Environ. Monit. Assess.* **191**, (2019).

25. Banger, K. *et al.* Terrestrial net primary productivity in India during 1901–2010: contributions from multiple environmental changes. *Clim. Change* **132**, 575–588 (2015).
26. Gahlot, S., Shu, S., Jain, A. K. & Baidya Roy, S. Estimating Trends and Variation of Net Biome Productivity in India for 1980–2012 Using a Land Surface Model. *Geophys. Res. Lett.* **44**, 11,573-11,579 (2017).
27. Asoka, A. & Mishra, V. Prediction of vegetation anomalies to improve food security and water management in India. *Geophys. Res. Lett.* **42**, 5290–5298 (2015).
28. Nayak, R. K., Patel, N. R. & Dadhwal, V. K. Inter-annual variability and climate control of terrestrial net primary productivity over India. *Int. J. Climatol.* **33**, 132–142 (2013).
29. US EPA. Climate change indicators in the United States 2016 Fourth Edition. *Evaluation* 663–670 (2016).
30. Ocean health index. SEA SURFACE TEMPERATURE. http://www.oceanhealthindex.org/methodology/component.
31. Zhu, Y. & Houghton, D. D. The impact of Indian Ocean SST on the large-scale Asian summer monsoon and the hydrological cycle. *Int. J. Climatol.* **16**, 617–632 (1996).
32. Schlich, R. The Indian Ocean: Aseismic Ridges, Spreading Centers, and Oceanic Basins BT - The Ocean Basins and Margins: The Indian Ocean. in (eds. Nairn, A. E. M. & Stehli, F. G.) 51–147 (Springer US, 1982). doi:10.1007/978-1-4615-8038-6_2.
33. Burns, J. M., Subrahmanyam, B. & Murty, V. S. N. On the dynamics of the Sri Lanka Dome in the Bay of Bengal. *J. Geophys. Res. Ocean.* **122**, 7737–7750 (2017).
34. Han, W. *et al.* Indian ocean decadal variability: A review. *Bull. Am. Meteorol. Soc.* **95**, 1679–1703 (2014).
35. Ashok, K., Guan, Z. & Yamagata, T. Influence of the Indian Ocean Dipole on the Australian winter rainfall. *Geophys. Res. Lett.* **30**, (2003).
36. Chowdary, J. S., Bandgar, A. B., Gnanaseelan, C. & Luo, J. J. Role of tropical Indian Ocean air-sea interactions in modulating Indian summer monsoon in a coupled model. *Atmos. Sci. Lett.* **16**, 170–176 (2015).
37. Ummenhofer, C. C., Sen Gupta, A., Li, Y., Taschetto, A. S. & England, M. H. Multi-decadal modulation of the El Nĩo-Indian monsoon relationship by Indian Ocean variability. *Environ. Res. Lett.* **6**, (2011).
38. Nayak, R. K., Patel, N. R. & Dadhwal, V. K. Spatio-temporal variability of net ecosystem productivity over India and its relationship to climatic variables. *Environ. Earth Sci.* **74**, 1743–1753 (2015).
39. Jha, S., Das, J. & Goyal, M. K. Assessment of Risk and Resilience of Terrestrial Ecosystem Productivity under the Influence of Extreme Climatic Conditions over India. *Sci. Rep.* **9**, 1–12 (2019).
40. Yamagata, T. *et al.* Coupled ocean-atmosphere variability in the tropical Indian ocean. *Geophys. Monogr. Ser.* **147**, 189–211 (2004).
41. Azad, S. & Rajeevan, M. Possible shift in the ENSO-Indian monsoon rainfall relationship under future global warming. *Sci. Rep.* **6**, 3–8 (2016).
42. Rao, A. S., Bala, G., Ravindranath, N. H. & Nemani, R. Multi-model assessment of trends, variability and drivers of terrestrial carbon uptake in India. *J. Earth Syst. Sci.* **128**, 1–19 (2019).
43. Shukla, J. & Fennessy, M. J. Simulation and Predictability of Monsoons. 567–575 (1994).
44. Prasanna, V. Impact of monsoon rainfall on the total foodgrain yield over India. *J. Earth Syst. Sci.* **123**, 1129–1145 (2014).
45. Deb Burman, P. K., Sarma, D., Chakraborty, S., Karipot, A. & Jain, A. K. The effect of Indian summer monsoon on the seasonal variation of carbon sequestration by a forest ecosystem over North-East India. *SN Appl. Sci.* **2**, 1–16 (2020).
46. Cherchi, A. *et al.* The influence of tropical Indian Ocean SST on the Indian summer monsoon. *J. Clim.* **20**, 3083–3105 (2007).
47. Jha, S., Sehgal, V. K., Raghava, R. & Sinha, M. Teleconnections of ENSO and IOD to summer monsoon and rice production potential of India. *Dyn. Atmos. Ocean.* **76**, 93–104 (2016).
48. Roxy, M. K. *et al.* Drying of Indian subcontinent by rapid Indian ocean warming and a weakening land-sea thermal gradient. *Nat. Commun.* **6**, (2015).
49. Costa de Oliveira, A., Marini, N. & Farias, D. R. *Climate Change: New Breeding Pressures and Goals*. *Encyclopedia of Agriculture and Food Systems* vol. 2 (Elsevier Ltd., 2014).

50. Osakabe, Y., Osakabe, K., Shinozaki, K. & Tran, L.-S. P. Response of plants to water stress. *Front. Plant Sci.* **5**, 86 (2014).
51. Singh, S. K., Reddy, V. R., Devi, M. J. & Timlin, D. J. Impact of water stress under ambient and elevated carbon dioxide across three temperature regimes on soybean canopy gas exchange and productivity. *Sci. Rep.* **11**, 1–13 (2021).
52. Valsala, V. *et al.* Intraseasonal variability of terrestrial biospheric CO2 fluxes over India during summer monsoons. *J. Geophys. Res. Biogeosciences* **118**, 752–769 (2013).
53. Sharma, A. & Goyal, M. K. District-level assessment of the ecohydrological resilience to hydroclimatic disturbances and its controlling factors in India. *J. Hydrol.* **564**, 1048–1057 (2018).
54. Xu, H. jie & Wang, X. ping. Effects of altered precipitation regimes on plant productivity in the arid region of northern China. *Ecol. Inform.* **31**, 137–146 (2016).
55. Zhu, Y., Luo, P., Zhang, S. & Sun, B. Spatiotemporal analysis of hydrological variations and their impacts on vegetation in semiarid areas from multiple satellite data. *Remote Sens.* **12**, 1–19 (2020).
56. Gornall, J. *et al.* Implications of climate change for agricultural productivity in the early twenty-first century. *Philos. Trans. R. Soc. B Biol. Sci.* **365**, 2973–2989 (2010).
57. Ji, Y. *et al.* Variation of net primary productivity and its drivers in China's forests during 2000–2018. *For. Ecosyst.* **7**, (2020).
58. Goswami, B. N., Krishnamurthy, V. & Annmalai, H. A broad-scale circulation index for the interannual variability of the Indian summer monsoon. *Q. J. R. Meteorol. Soc.* **125**, 611–633 (1999).
59. Roy, P. S. *et al.* New vegetation type map of India prepared using satellite remote sensing: Comparison with global vegetation maps and utilities. *Int. J. Appl. Earth Obs. Geoinf.* **39**, 142–159 (2015).
60. Ahmad, L., Habib Kanth, R., Parvaze, S. & Sheraz Mahdi, S. Agro-climatic and Agro-ecological Zones of India BT - Experimental Agrometeorology: A Practical Manual. in (eds. Ahmad, L., Habib Kanth, R., Parvaze, S. & Sheraz Mahdi, S.) 99–118 (Springer International Publishing, 2017). doi:10.1007/978-3-319-69185-5_15.
61. Parthasarathy, B., Kumar, K. R. & Kothawale, D. R. Indian summer monsoon rainfall indices: 1871-1990. *Meteorol. Mag.* **121**, 174–186 (1992).
62. Li, X. & Xiao, J. A global, 0.05-degree product of solar-induced chlorophyll fluorescence derived from OCO-2, MODIS, and reanalysis data. *Remote Sens.* **11**, (2019).
63. Li, X. *et al.* Solar-induced chlorophyll fluorescence is strongly correlated with terrestrial photosynthesis for a wide variety of biomes: First global analysis based on OCO-2 and flux tower observations. *Glob. Chang. Biol.* **24**, 3990–4008 (2018).
64. Xiao, J. *et al.* Solar-induced chlorophyll fluorescence exhibits a universal relationship with gross primary productivity across a wide variety of biomes. *Glob. Chang. Biol.* **25**, e4–e6 (2019).
65. Huang, B. *et al.* Improvements of the Daily Optimum Interpolation Sea Surface Temperature (DOISST) Version 2.1. *J. Clim.* **34**, 2923–2939 (2021).
66. Banzon, V., Smith, T. M., Mike Chin, T., Liu, C. & Hankins, W. A long-term record of blended satellite and in situ sea-surface temperature for climate monitoring, modeling and environmental studies. *Earth Syst. Sci. Data* **8**, 165–176 (2016).
67. Hersbach, H. *et al.* The ERA5 global reanalysis. *Q. J. R. Meteorol. Soc.* **146**, 1999–2049 (2020).
68. Rayner, N. A. *et al.* Global analyses of sea surface temperature, sea ice, and night marine air temperature since the late nineteenth century. *J. Geophys. Res. Atmos.* **108**, (2003).
69. Saji, N. H. & Yamagata, T. Possible impacts of Indian Ocean Dipole mode events on global climate. *Clim. Res.* **25**, 151–169 (2003).
70. Amy McNally NASA/GSFC/HSL (2018). FLDAS Noah Land Surface Model L4 Global Monthly 0.1 x 0.1 degree (MERRA-2 and CHIRPS) (Version 001) [Dataset], Greenbelt, Maryland, USA, Goddard Earth Sciences Data and Information Services Center (GES DISC). (2018) doi:10.5067/9JBLK69HNL3V.
71. Gelaro, R. *et al.* The modern-era retrospective analysis for research and applications, version 2 (MERRA-2). *J. Clim.* **30**, 5419–5454 (2017).

Figures

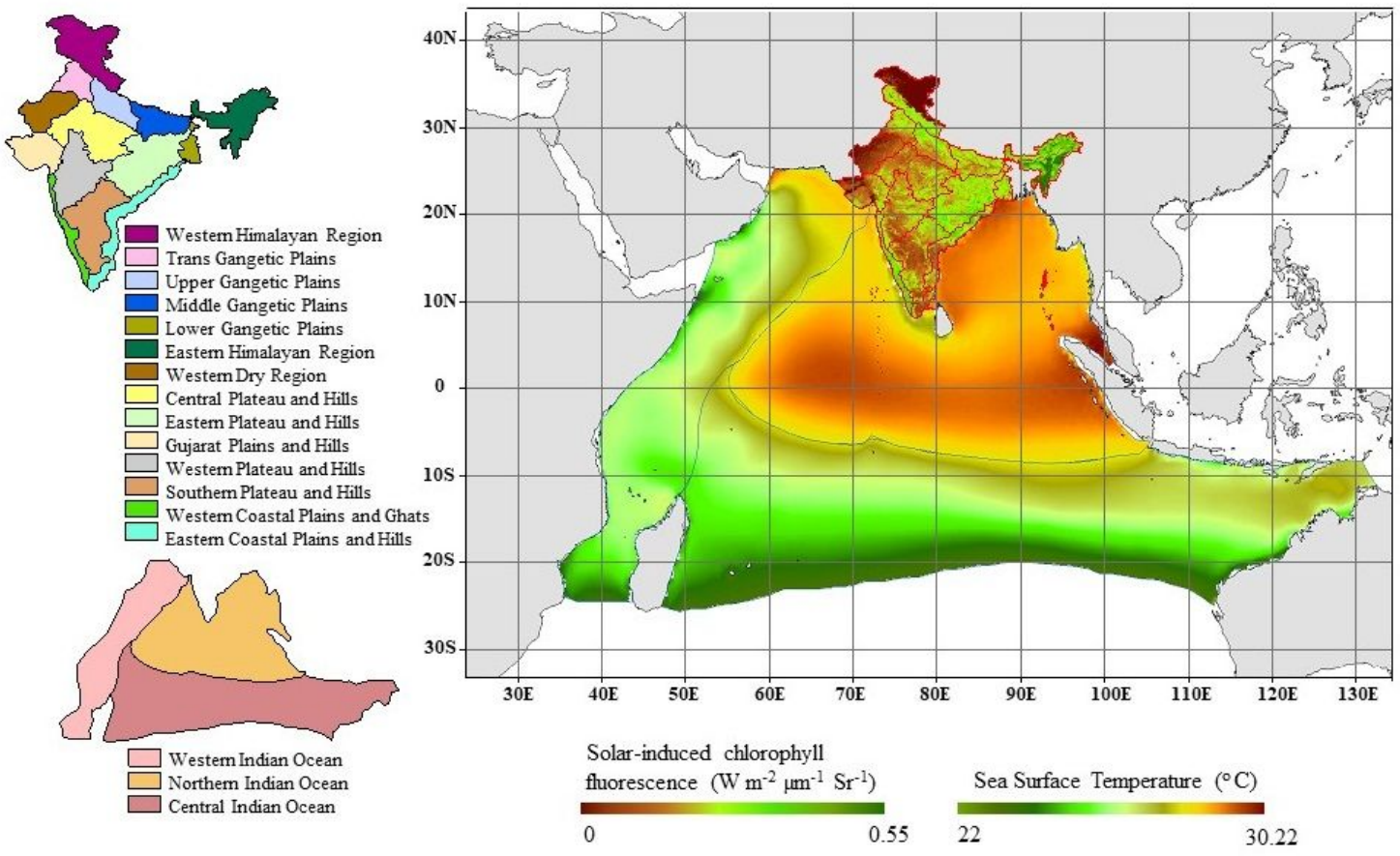

Figure 1

Study area showing the Indian landmass with 14 agro-climatic zones (Upper LH) and the Indian sub-continent with the Indian Ocean stratified into Western, Northern, and Central regions based on the SST pattern (Lower LH). The climatology of SIF and SST during summer monsoon season is shown for the period of 2001 to 2018 (RH).

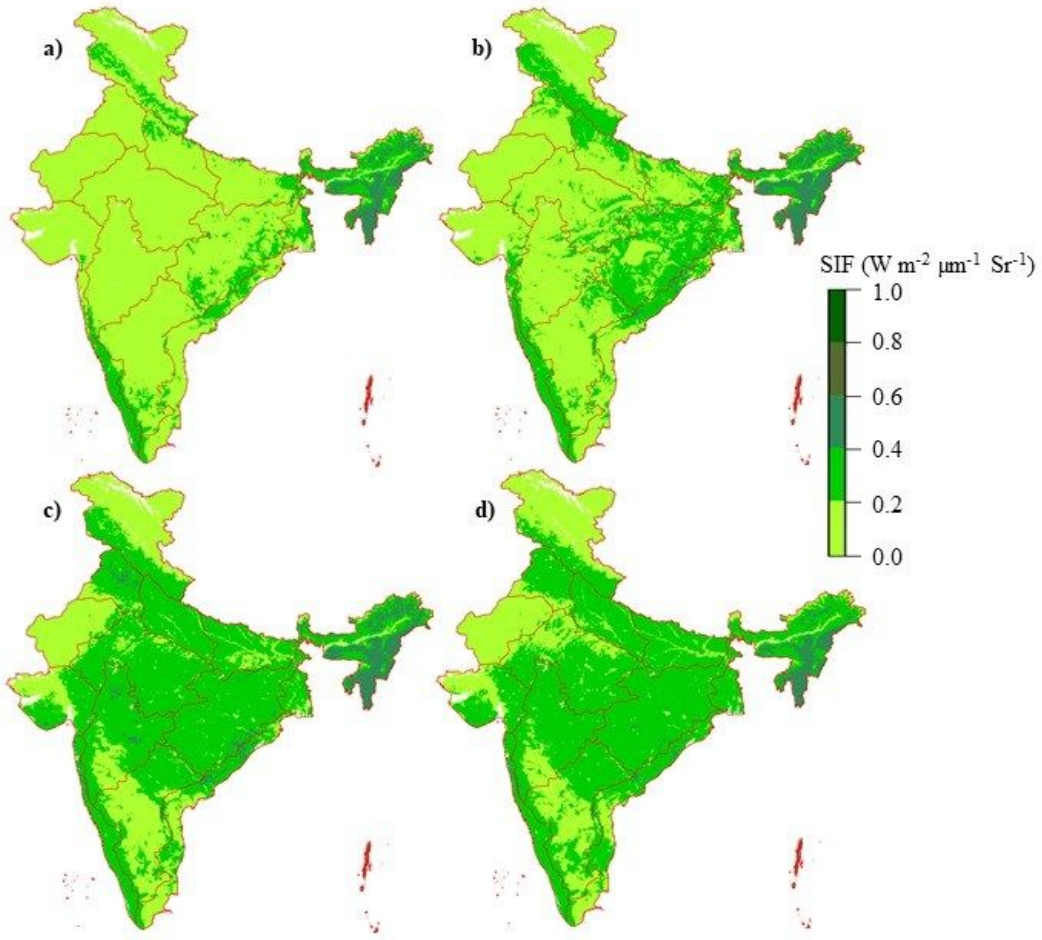

Figure 2

Spatial variation of mean SIF (W m-2 µm-1 Sr-1) across India during the months of a) June, b) July, c) August, and d) September indicates progressive increase from June to September with respect to growing season. The regions with higher SIF values during the month of June indicates presence of forest and natural vegetation.

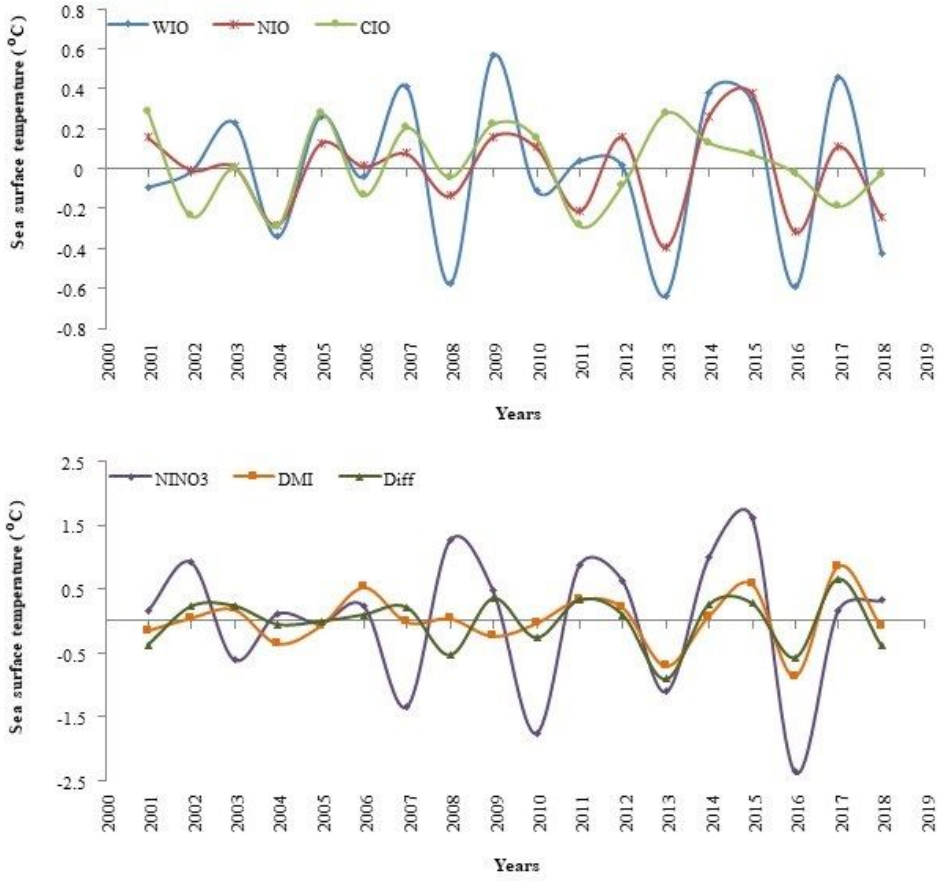

Figure 3

Time series of basin wise average SST anomalies over a) Western Indian Ocean, North Indian Ocean and Central Indian Ocean, and time series of b) NINO3 SST anomalies, DMI and W-CIO index during monsoon season (2001- 2018), which depicts a strong interannual variability.

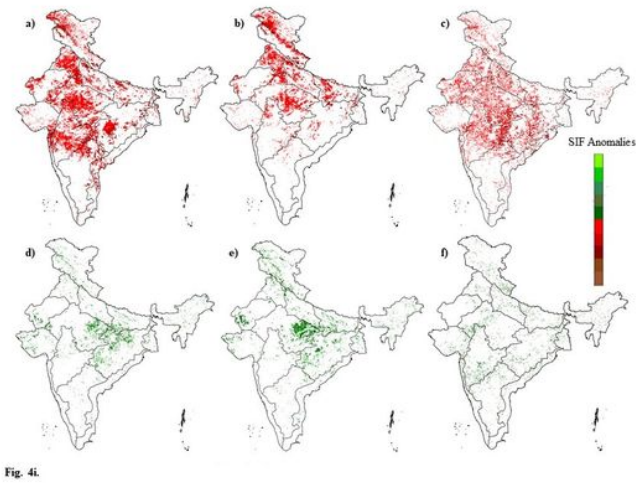

Fig. 4i.

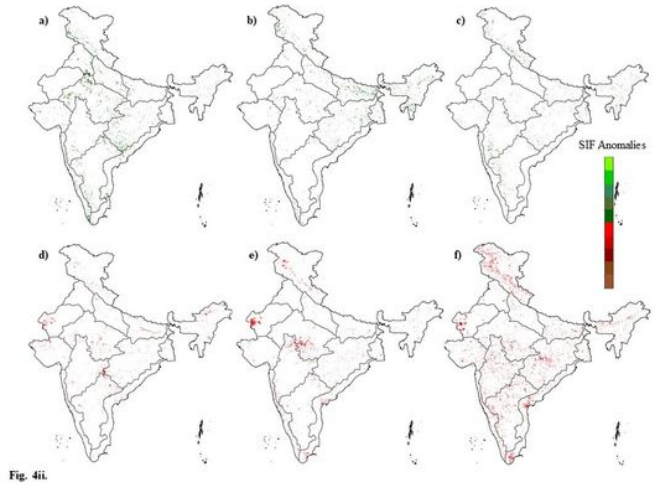

Fig. 4ii.

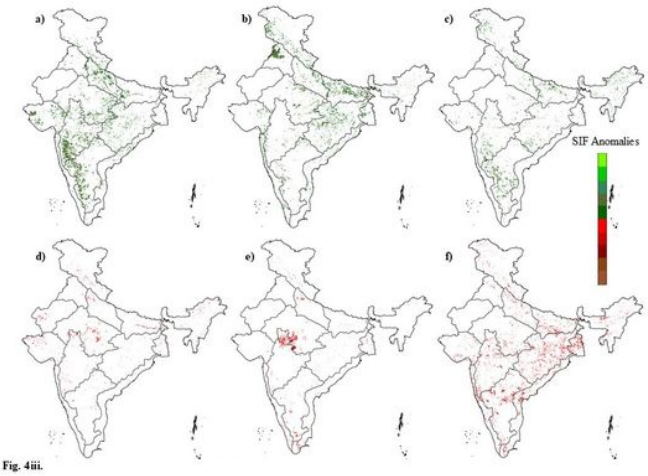

Fig. 4iii.

Figure 4

4i. Composite anomalies of SIF (W m-2 µm-1 Sr-1) across India during the month of June when, SST anomalies of the Western Indian Ocean (a,d), Northern Indian Ocean (b,e), and Central Indian Ocean (c,f) demonstrated positive (upper) and negative (lower) trends. The warmer SST in the Oceanic regions lead to negative SIF anomalies (red), while colder SST leads to positive SIF anomalies (green) 4ii. Composite anomalies of SIF (W m-2 µm-1 Sr-1) across India during the month of August when, SST anomalies of the Western Indian Ocean (a,d), Northern Indian Ocean (b,e), and Central Indian Ocean (c,f) demonstrated positive (upper) and negative (lower) trends. The warmer SST in the Oceanic regions lead to positive SIF anomalies (red), while colder SST leads to negative SIF anomalies (green) 4iii. Composite anomalies of SIF (W m-2 µm-1 Sr-1) across India during the month of September when, SST anomalies of the Western Indian Ocean (a,d), Northern Indian Ocean (b,e), and Central Indian Ocean (c,f) demonstrated positive (upper) and negative (lower) trends. The warmer SST in the Oceanic regions lead to positive SIF anomalies (red), while colder SST leads to negative SIF anomalies (green)

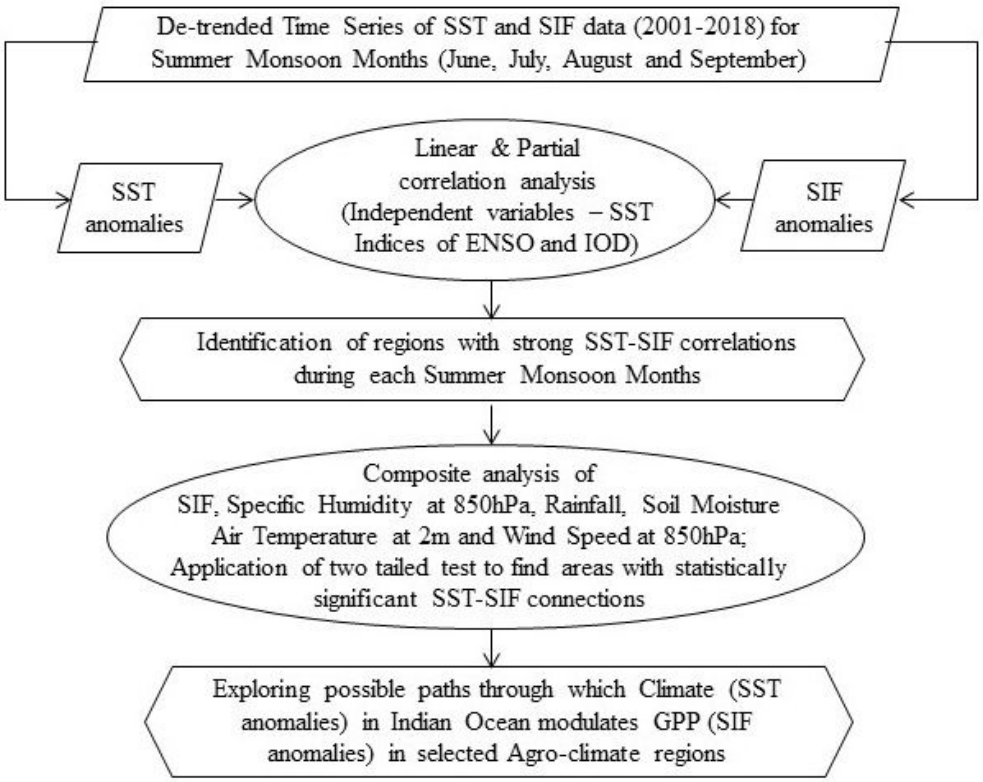

Figure 5

Methodology Flow Diagram with various steps followed for establishing relationship between Climate and Primary Productivity in the Indian sub-continent region

Supplementary Files

This is a list of supplementary files associated with this preprint. Click to download.

- Figuressupplementarysstsif.pdf
- Tablessupplementarysstsif.docx